^{64}Cu-Azabicyclo[3.2.2]Nonane Thiosemicarbazone Complexes: Radiopharmaceuticals for PET of Topoisomerase II Expression in Tumors

Lihui Wei[1], Johnny Easmon[2], Ravneet K. Nagi[1], Brian D. Muegge[1], Laura A. Meyer[1], and Jason S. Lewis[1]

[1]*Division of Radiological Sciences, Mallinckrodt Institute of Radiology, and Alvin J. Siteman Cancer Center, Washington University School of Medicine, St. Louis, Missouri; and* [2]*Institute of Pharmacy, University of Innsbruck, Innsbruck, Austria*

Topoisomerase II (Topo-II) is an essential enzyme in the DNA replication process and is the primary cellular target for many of the most widely used and effective anticancer agents. It has been reported that thiosemicarbazones (TSCs) are potent antitumor agents that inhibit Topo-II. The aim of this study was to investigate the relationship between the in vitro and in vivo behavior of novel ^{64}Cu-TSC complexes and the expression of Topo-II activity. **Methods:** Four ^{4}*N*-azabicyclo[3.2.2]nonane TSC derivatives (EPH142, EPH143, EPH144, and EPH270) were successfully radiolabeled with ^{64}Cu, to form lipophilic cations of the general formula [^{64}Cu(L)]Cl, and the partition coefficient (logP) values were determined. One agent [^{64}Cu-EPH270]$^{+}$ was observed in vitro in cultured cell studies. The kinetics of 2 compounds, [^{64}Cu-EPH144]$^{+}$ and [^{64}Cu-EPH270]$^{+}$, were examined in mice bearing L1210 tumors and small-animal PET was conducted in mice bearing L1210 and PC-3 tumors, which expressed high and low levels of Topo-II, respectively. All data were compared with the activity and levels of Topo-II, as determined by a commercially available assay kit and western blot analysis. **Results:** The 4 complexes were radiolabeled by incubation of $^{64}CuCl_2$ with the ligand in ethanolic solution. The complexes were isolated in high radiochemical purity, as determined by radio–thin-layer chromatography and radio–high-performance liquid chromatography. The compounds were shown to be lipophilic with logP values ranging from 1.34 to 1.92. In biodistribution studies, good L1210 tumor uptake was noted ([^{64}Cu-EPH144]$^{+}$ at 1 h, 4.70 %ID/g [percentage injected dose per gram]; 4 h, 8.80 %ID/g; 24 h, 6.64 %ID/g; and [^{64}Cu-EPH270]$^{+}$ at 1 h, 2.58 %ID/g; 4 h, 6.00 %ID/g; 24 h, 4.80 %ID/g). Small-animal PET of animals with L1210 tumors (high Topo-II expressing) showed excellent tumor accumulation compared with that of animals with PC-3 tumors (low Topo-II expressing), and the L1210 tumor uptake was significantly reduced by coadministration of a Topo-II poison. **Conclusion:** Here we describe the characterization of a new class of copper-radiolabeled TSC analogs. We demonstrate that the accumulation of the ^{64}Cu-compounds is related to the expression levels of Topo-II in tumor tissue.

Key Words: small-animal PET; ^{64}Cu; topoisomerase-II; thiosemicarbazones

J Nucl Med 2006; 47:2034–2041

The use of copper-thiosemicarbazone (TSC) complexes for use in PET has been avidly explored because of the increasing availability and dissemination of the positron-emitting nuclides of copper: ^{60}Cu (half-life [$t_{1/2}$] = 0.40 h, β^{+} = 93%, electron capture [EC] = 7%); ^{61}Cu ($t_{1/2}$ = 3.32 h, β^{+} = 62%, EC = 38%); ^{62}Cu ($t_{1/2}$ = 0.16 h, β^{+} = 98%, EC = 2%); and ^{64}Cu ($t_{1/2}$ = 12.7 h, β^{+} = 17.4%, EC = 43%) (*1–4*). The basic science and clinical exploration of copper-TSC moieties is separated into 2 distinct classes of agents: those used to determine blood flow (*5–7*) and those used to demonstrate the presence of hypoxia in tissue (*8–13*). When complexed with a larger amount of ^{64}Cu, copper-TSC agents have also been described as potential radiotherapeutics on the basis of their biologic and nuclear properties (*14–16*).

Topoisomerase II (Topo-II) is a 170-kDa nuclear protein found in eukaryotic cells that decatenates or disentangles DNA coils, passing one helix through another to prevent supercoiling during DNA replication (*17,18*). Topo-II requires energy in the form of adenosine triphosphate (ATP) and functions by generating transient double-stranded DNA breaks while preserving the integrity of the genetic material through a protein bridge that spans the break. The DNA–Topo-II complex, also known as a cleavage complex, is generally tolerated in small quantities by cells; large quantities of the cleavage complexes may cause frame-shift mutations, permanent double-stranded DNA breaks, undesirable recombination, and apoptosis (*17*).

Because Topo-II is necessary for DNA synthesis and cellular division, rapidly proliferating cells—such as tumors—generally contain high levels of this enzyme. In transformed cells, the cellular levels of Topo-II increase (~5-fold) during the cell cycle, peaking before mitosis (*19,20*). This is followed by a sharp decrease during the G_1 phase, maintaining very low levels (undetectable) until the early

Received Jul. 25, 2006; revision accepted Sep. 5, 2006.

For correspondence or reprints contact: Jason S. Lewis, PhD, Mallinckrodt Institute of Radiology, Washington University School of Medicine, 510 S. Kingshighway Blvd., Campus Box 8225, St. Louis, MO 63110.

E-mail: j.s.lewis@wustl.edu

G_0 phase (*19,21*). The fact that Topo-II is rapidly lost on completion of mitosis confirms that the enzyme is a specific and sensitive marker for cell proliferation (*20,21*). Topo-II is closely regulated in normal cells, but tumors maintain high levels of Topo-II (*22*), making Topo-II a target for several antitumor agents (*17,18,23–27*). Topo-II expression has also been associated with chemosensitivity to cytotoxic agents, and a clear relationship exists between qualitative alterations of Topo-II and drug sensitivity in a series of in vitro biologic systems (*27,28*). However, the clinical relevance of these drug sensitivity interactions remains controversial. Also, the control mechanism for Topo-II expression is unknown, as is its relationship to cell survival when absent (*27*). Therefore, developing methods to systematically explore Topo-II expression in tumors in noninvasive assays to predict drug efficacy in human cancers is attractive.

Several groups have investigated TSCs as antitumor agents and have shown that these agents inhibit Topo-II expression (*29–34*), acting by stabilization of the cleavable products formed by Topo-II and DNA (*34,35*). Copper-TSC complexes have significantly higher growth inhibitory activity than the uncomplexed ligand and have lower IC_{50} (inhibitory concentrations of 50%) values against tumor cells than other reported Topo-II inhibitors (*29*). Taking advantage of the availability of positron-emitting nuclides of copper, we undertook the radiolabeling of 4 new TSC derivatives (EPH142, EPH143, EPH144, and EPH270) with ^{64}Cu and examined the structure–activity relationships of these compounds in animal tumor models. In this report we describe the radiolabeling of 4 TSCs (Fig. 1), characterization of the agents and the biologic kinetics, and small-animal PET of the lead compounds in 2 mouse tumor models confirmed to express high and low levels of Topo-II.

MATERIALS AND METHODS

Materials

^{64}Cu was produced on a CS15 cyclotron (Cyclotron Corp.) at Washington University School of Medicine by previously reported methods (*2*). Unless otherwise stated, all chemicals (including VP-16) were purchased from Sigma-Aldrich Chemical Co., Inc. Thin-layer chromatography (TLC) plates were analyzed on a BIOSCAN System 200 imaging scanner. Radioactive samples were counted on a Beckman 8000 γ-counter. Female CDF1 mice, 11 wk old, and male *nu/nu* mice, 5–6 wk old, were purchased from Charles River Laboratories. L1210 (mouse lymphocytic leukemia), LL/2 (mouse Lewis lung carcinoma), B16F10 (mouse melanoma), EMT-6 (mouse mammary carcinoma), CaSki (human cervix epidermoid carcinoma), MCF-7 (human breast adenocarcinoma), and PC-3 (human prostate adenocarcinoma) cells were purchased from the American Type Culture Collection and maintained in our laboratories by serial cell culture. To determine the activity of Topo-II in both cultured cells and tumors, a qualitative assay was performed using a commercially available kit from TopoGEN, Inc., per manufacturer's instructions. Western blot analysis was performed to determine the cellular levels of Topo-II. Protein content in cells and in tumor extracts was determined using a BCA Protein Assay Kit (Pierce Chemicals). Nonradioactive analogs ([Cu(L)]Cl), to serve as standards, were synthesized and characterized according to previously published methods (*29*). These nonradioactive analogs were used as standards in both radio-TLC and radio–high-performance liquid chromatography (radio-HPLC) identification of radiochemical purity.

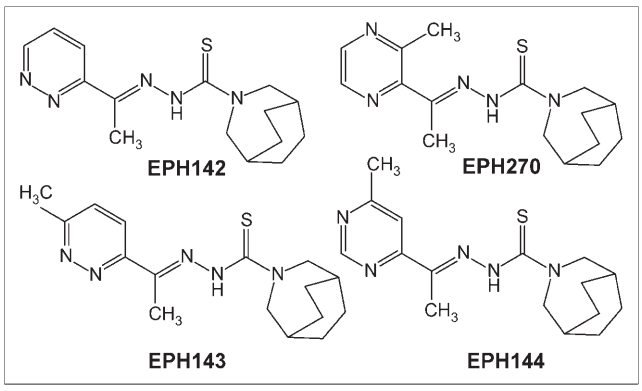

FIGURE 1. Structures of ligands (L) EPH142, EPH143, EPH144, and EPH270, the four ^{4}*N*-azabicyclo[3.2.2]nonane TSC derivatives labeled with ^{64}Cu to form complexes of the general formula $[Cu\text{-}L]^+$ (*29*), whose identity was confirmed by chromotographic comparison with nonradioactive standards.

Radiochemistry and Lipophilicity Studies

The ligands were manufactured as previously reported (*29*) and were dissolved in ethanol at 1 mg/mL, to form a yellow solution. $^{64}CuCl_2$ (18.5–185.0 MBq [0.5–5 mCi]) was taken up into 150 μL ethanol, and 5 μL of the ligand ethanolic solution were added. The reaction mixture was heated at 40°C for 1 h. Radiochemical purity was determined by TLC using Silica Gel TLC plates (EM Merck) with 60:40 acetonitrile:0.9% saline as the mobile phase (free ^{64}Cu: $R_f = 0$; ^{64}Cu-complexes: $R_f = 0.9$). Radiochemical purity was also confirmed by radio-HPLC methods (solvent A: 0.025 mol/L phosphate buffer, pH 4.0; solvent B: acetonitrile; gradient = 20%–70% B in 8 min; flow rate, 2 mL/min; Phenomex LUNA C_{18} column).

The octanol–water partition coefficient was used as a measure of lipophilicity. The radiotracer solution (20 μL) was added to a mixture of phosphate-buffered saline (PBS, pH 7.4) (500 μL) and *n*-octanol (500 μL) in a microcentrifuge tube. After vortexing for 5 min, the tube was centrifuged (5 min at 3,000 rpm) and 100-μL samples of each layer were taken for counting. All experiments were performed in triplicate. The partition coefficient was expressed as $\log P = \log_{10}$(counts in octanol/counts in PBS).

Topo-II Enzyme Assays

TopoGEN Kit. The kit is designed to ascertain Topo-II activity in cell extracts. Following the instructions included with the kit, equal amounts of tissue (μg protein) were added to the reaction buffer containing ATP, required for Topo-II function, and a kintoplast DNA (kDNA) substrate, which is a collection of interlocking circles that only Topo-II can decatenate. In general, cultured cells or tumors were harvested and were homogenized and their nuclear extracts were aliquoted and stored at −80°C after their protein content was determined using a standard BCA Protein Assay Kit.

A separate study was also undertaken to compare the effect of the Cu-azabicyclo[3.2.2]nonane TSCs—specifically, nonradioactive

Cu-EPH270—on the level of Topo-II–mediated decatenization of the kDNA to establish Cu-EPH270 as a Topo-II poison. Following the TopoGEN kit instructions, Topo-II (2 units/20 μL), VP-16 as a positive control (1 mmol/L), and nonradioactive Cu-EPH270 (1 mmol/L) were incubated at 37°C for 30 min, during which time the Topo-II in the samples decatenized the kDNA substrate. The reactions were then loaded onto a 1% agarose gel with ethidium bromide (0.5 μg/mL) for electrophoresis. Photographs of the gels were taken with an ultraviolet transilluminator.

Western Blot. Cellular extracts or nuclear protein extracts from harvested tumors were solubilized in Laemmli's buffer and were loaded onto a 7.5% sodium dodecyl sulfate (SDS)-polyacrylamide gel and run for 1 h at 150 V. Separated proteins were transferred to polyvinylidene difluoride membranes (BioRad Laboratories) in a BioRad Trans Blot Cell using a buffer containing 25 nmol/L Tris-Cl, 86 mmol/L glycine, and 20% methanol. To avoid nonspecific binding, the membranes were blocked with 5% nonfat dry milk in 0.05% Tween-20 in Tris-buffered saline for 30 min. The membranes were then incubated with primary antibody diluted in blocking buffer. A rabbit polyclonal antibody prepared against a 16-residue oligopeptide derived from the carboxyl-terminal region of human Topo-IIα (TopoGEN, Inc.) was used at a dilution of 1:1,000. After binding, the blots were washed and incubated with goat antirabbit horseradish peroxidase–conjugated secondary antibody. The protein-antibody complexes were visualized by enhanced chemoluminescence (ECL system; Amersham) according to the manufacturer's protocol. The positions of Topo-IIα were localized by human 170-kDa Topo-IIα marker (TopoGEN, Inc.).

In Vitro Studies

A cell uptake study of $[^{64}Cu\text{-}EPH270]^+$ was performed with the B16F10 cell line to investigate the effect of varying the mass of $[Cu\text{-}EPH270]^+$ against cell uptake and retention. Different amounts of $[^{64}Cu\text{-}EPH270]^+$ were incubated with B16F10 cells in 6-well plates at 37°C for 1 h. After washing with PBS buffer, the cells were lysed with SDS solution and counted with a γ-counter. The amount of activity associated with the cells was normalized for protein content.

In Vivo Studies

Female CDF1 mice were implanted subcutaneously with 5.0×10^5 L1210 cells from cell culture into the mouse flank. At 12 d of tumor growth (tumors, ~1.3 g), $[^{64}Cu\text{-}EPH144]^+$ or $[^{64}Cu\text{-}EPH270]^+$ (0.26 MBq [7 μCi] in 150 μL 0.9% saline, >99% radiochemical purity) was injected via tail vein, and the animals were euthanized at 1, 4, and 24 h ($n = 5$ for each time point). Selected tissues and organs were harvested and weighed and the activity was counted on the γ-counter. The percentage injected dose per gram (%ID/g) and the percentage injected dose per organ (%ID/organ) were calculated for each tissue.

All imaging was performed in a temperature-controlled imaging suite with close monitoring of the physiologic status of the animals. Athymic nude (*nu/nu*) mice were implanted with either 5.0×10^5 L1210 cells or 3×10^6 PC-3 cells into the flank. Small-animal PET was performed on a microPET FOCUS system (Siemens Medical Solutions USA, Inc.) (*36*). Male *nu/nu* mice bearing 12-d L1210 tumors or 21-d PC-3 tumors ($n = 6$ per group) were anesthetized with 1%–2% isoflurane, placed in a supine position, and immobilized in a custom-made cradle. The mice received 7.4 MBq (200 μCi) of $[^{64}Cu\text{-}EPH270]^+$ via the tail vein and were imaged side by side with mice that had been pretreated with 100 μg of VP-16 in 150 μL 0.9% saline immediately before injection of $[^{64}Cu\text{-}EPH270]^+$. Animals were imaged with a 10-min static data collection at 1, 4, and 24 h after injection. Standard uptake values (SUVs) were generated from regions of interest drawn over the tumor and other organs of interest. Coregistration of the PET images was achieved in combination with a microCAT-II camera (Imtek Inc.), which provides high-resolution CT anatomic images. The image registration between microCT and PET images was accomplished by using a landmark registration technique, AMIRA image display software (AMIRA; TGS Inc.). The registration method proceeds by rigid transformation of the microCT images from landmarks provided by fiducial markers directly attached to the animal bed.

Statistical Methods

To compare differences between the datasets, a Student *t* test was performed. Differences at the 95% confidence level ($P < 0.05$) were considered significant.

RESULTS

Radiochemistry and Lipophilicity Studies

All 4 ligands were radiolabeled with ^{64}Cu in ethanolic solution at 40°C for 1 h to yield >95% radiochemical purity. The ^{64}Cu-labeled complexes were obtained in specific activities of 3.7–37 MBq/μg (0.1–1.0 mCi/μg). Radio-TLC on Silica Gel plates (with coelution of the nonradioactive analog, [Cu(L)]Cl) demonstrated the isolation of radiochemically pure compounds ($^{64}CuCl_2$, $R_f = 0.0$ [100%]; $[^{64}Cu\text{-}EPH142]^+$ = 1 peak, $R_f = 0.9$ [100%]; $[^{64}Cu\text{-}EPH143]^+$ = 1 peak, $R_f = 0.9$ [98%]; $[^{64}Cu\text{-}EPH144]^+$ = 1 peak, $R_f = 0.9$ [98%]; $[^{64}Cu\text{-}EPH270]^+$ = 1 peak, $R_f = 0.9$ [98%]). Radio-HPLC confirmed radiochemical purities of >98% for all 4 complexes ($[^{64}Cu\text{-}EPH142]^+$ = 1 peak, retention time [t_R] = 10.0 min; $[^{64}Cu\text{-}EPH143]^+$ = 1 peak, $t_R = 10.2$ min; $[^{64}Cu\text{-}EPH144]^+$ = 1 peak, $t_R = 10.05$ min; $[^{64}Cu\text{-}EPH270]^+$ = 1 peak, $t_R = 10.25$ min). The HPLC retention times of the complexes were confirmed to be identical to those of the nonradioactive analogs, by coelution of the nonradioactive standards with their respective radioactive analogs. The standards were previously identified and confirmed to be monocationic species of the general formula $[Cu(L)]^+$. The partition coefficients of the four ^{64}Cu-complexes were determined by octanol:PBS partition experiments. The logP values ± SD obtained were 1.72 ± 0.18 ($[^{64}Cu\text{-}EPH142]^+$), 1.33 ± 0.16 ($[^{64}Cu\text{-}EPH143]^+$), 1.92 ± 0.18 ($[^{64}Cu\text{-}EPH144]^+$), and 1.34 ± 0.21 ($[^{64}Cu\text{-}EPH270]^+$).

Topo-II Enzyme Assays

Examination of tumor extracts with the TopoGEN assay kit demonstrates different amounts of Topo-II in the tumor extracts (Fig. 2A), confirming the ability to determine the relative Topo-II activity in tumors. As seen by the bands on the gel, the order of Topo-II activity in these tumor lines was LL/2 > PC-3 > MCF-7. Western blot analysis of cellular extracts from harvested L1210, LL/2, PC-3, and MCF-7 tumors (Fig. 2B) showed different levels of Topo-II protein (L1210 > LL/2 > PC-3 > MCF-7). The results from the western blot analysis are consistent with the

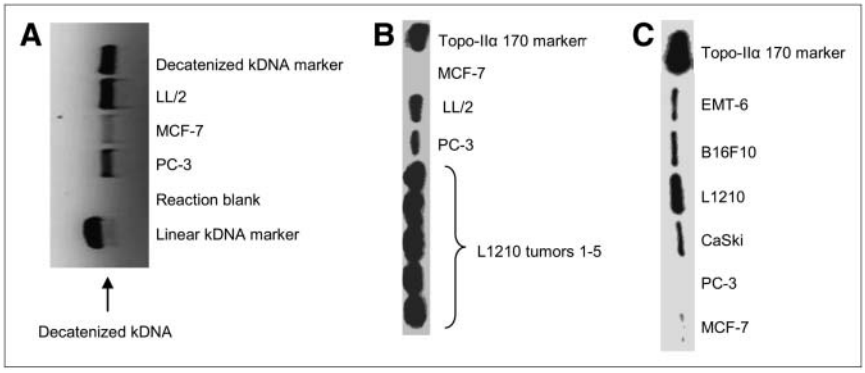

FIGURE 2. (A) Topo-II activity was measured by production of decatenized kDNA; more Topo-II activity corresponds to a more optically dense decatenized kDNA band in an agarose gel. Any bands that line up with the linear kDNA marker are indicative of kDNA degradation by nucleases. No bands line up with this marker, meaning there was no such degradation. The reaction blank, kDNA without tumor extract, indicates that bands produced by the reactions are not due to contamination. As seen by the bands on this gel, the order of Topo-II activity in these tumor lines was LL/2 > PC-3 > MCF-7. (B) Western blot analysis of proteins prepared from nuclear extracts from L1210, LL/2, PC-3, and MCF-7 tumors. Nuclear proteins (5 μg) were size fractionated electrophoretically, transferred to a membrane, incubated with antibody against Topo-IIα, and visualized by chemoluminescence. 170 marker = 170-kDa marker. (C) Western blot analysis of proteins prepared from cellular extracts from L1210, EMT-6, B16F10, CaSki, PC-3, and MCF-7 cell lines.

Topo-II assay, indicating that more Topo-II protein (western blot) corresponds to higher Topo-II activity (Topo-II assay). Figure 2B shows the levels of Topo-II from L1210 tumors harvested from 5 mice. The results indicate that the tumors grown in different mice yield the same amounts of Topo-II. To determine which cell lines to use for the in vivo studies, a western blot experiment was performed on cellular extracts from 6 cell lines, and the results are presented in Figure 2C. In culture, L1210 cells demonstrate the highest level of Topo-II, followed by B16F10, EMT-6, and CaSki cell lines, whereas MCF-7 and PC-3 cells have the lowest amount of Topo-II expression.

To confirm selective inhibition of Topo-II by nonradioactive Cu-EPH270, reactions comparing its effect with that of VP-16 (positive control) were conducted (Fig. 3). Although the Cu-EPH270 proved to be somewhat insoluble, its solubility improved after storing it in the solvent for additional time. Optimization of the procedure for appropriate concentrations of Topo-II (2 units/20 μL), VP-16, and Cu-EPH270 produced evidence that Cu-EPH270 acted as an inhibitor of Topo-II.

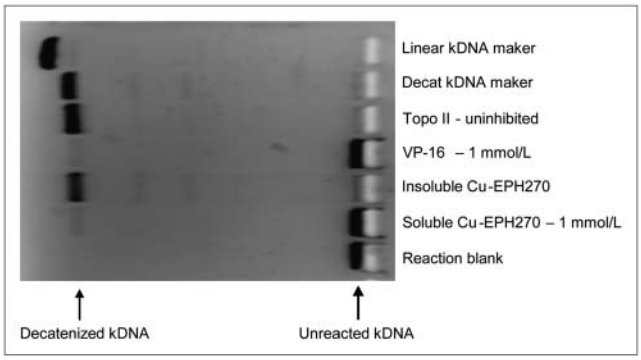

FIGURE 3. This experiment demonstrates that VP-16 and soluble nonradioactive Cu-EPH270 both inhibit Topo-II activity, as no bands of decatenized (decat) kDNA are produced for those wells. The reaction blank indicates that bands produced by the reactions are not due to contamination.

In Vitro Studies

We undertook a dose–response experiment by varying the Cu-TSC mass against cell uptake. A relationship between the mass of $[^{64}Cu\text{-}EPH270]^+$ given and its in vitro uptake into the B16F10 cell line was observed (Fig. 4). As the mass of $[^{64}Cu\text{-}EPH270]^+$ added to the cells was increased, the cellular uptake of the compound increased correspondingly until a mass was achieved that resulted in saturation and then gradual decrease in uptake was noted. These observations strongly suggest that a process based on dose–response is responsible for the accumulation and retention of the Cu-TSC complex in this cell line.

In Vivo Studies

A summary of the biodistribution data obtained in L1210-bearing mice for both $[^{64}Cu\text{-}EPH144]^+$ and $[^{64}Cu\text{-}EPH270]^+$ is given in Table 1. Both $[^{64}Cu\text{-}EPH144]^+$ and $[^{64}Cu\text{-}EPH270]^+$ remained relatively high in the blood,

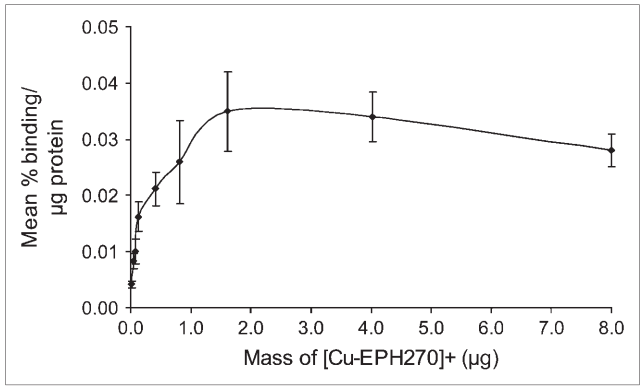

FIGURE 4. Relationship between the mass of $[^{64}Cu\text{-}EPH270]^+$ administered and its in vitro uptake into B16F10 cell line was observed. As the mass of Cu-EPH270 added to cells was increased, cellular uptake of the compound increased until a mass was achieved that resulted in a plateau and in a gradual decrease in uptake. These observations strongly suggest that a process based on dose–response was responsible for accumulation of $[^{64}Cu\text{-}EPH270]^+$ into different cell lines.

TABLE 1
Biodistribution (%ID/g ± SD, $n = 5$) at 1, 4, and 24 Hours of $[^{64}Cu\text{-}EPH144]^+$ and $[^{64}Cu\text{-}EPH270]^+$ in CFD1 Mice Bearing Lymphocytic Leukemia L1210 Tumors

Biodistribution	Time (h)		
	1	4	24
	$[^{64}Cu\text{-}EPH144]^+$		
Blood	5.03 ± 0.46	4.04 ± 0.41	2.58 ± 0.43
Lung	24.36 ± 7.60	20.38 ± 5.53	14.49 ± 2.89
Liver	39.95 ± 7.06	34.57 ± 8.01	22.11 ± 5.16
Spleen	15.02 ± 3.30	11.75 ± 1.46	8.42 ± 1.17
Kidney	24.32 ± 2.73	15.79 ± 1.84	12.92 ± 2.98
Muscle	2.06 ± 0.48	1.60 ± 0.41	1.34 ± 0.30
Fat	1.38 ± 0.33	1.01 ± 0.40	0.62 ± 0.24
Heart	14.29 ± 1.70	11.66 ± 2.35	9.87 ± 2.21
Bone	2.71 ± 0.58	2.66 ± 0.40	2.50 ± 1.16
Tumor	4.70 ± 0.47	8.80 ± 1.94	6.64 ± 1.30
	$[^{64}Cu\text{-}EPH270]^+$		
Blood	3.69 ± 1.69	5.14 ± 1.20	3.05 ± 0.58
Lung	19.40 ± 14.20	27.14 ± 6.02	14.87 ± 4.03
Liver	20.15 ± 11.90	28.01 ± 5.57	18.41 ± 4.45
Spleen	6.17 ± 4.10	10.46 ± 2.90	6.53 ± 2.13
Kidney	16.45 ± 6.06	14.35 ± 5.62	11.10 ± 1.95
Muscle	1.01 ± 0.54	1.11 ± 0.28	1.06 ± 0.25
Fat	0.61 ± 0.26	1.11 ± 0.48	0.38 ± 0.34
Heart	5.23 ± 3.27	9.08 ± 1.63	7.43 ± 1.74
Bone	2.91 ± 3.97	1.94 ± 0.76	1.52 ± 0.56
Tumor	2.58 ± 1.42	6.00 ± 0.75	4.80 ± 0.89

with low clearance over the 24-h period ($[^{64}Cu\text{-}EPH144]^+$, 5.03 %ID/g at 1 h vs. 2.58 %ID/g at 24 h; $[^{64}Cu\text{-}EPH270]^+$, 3.69 %ID/g at 1 h vs. 3.05 %ID/g at 24 h). Both compounds also had high levels of uptake in the lung, spleen, kidney, and liver at 1 h, but activity in these tissues decreased over 24 h. The heart uptake of both agents was high at all time points and similar at 24 h after injection ($[^{64}Cu\text{-}EPH144]^+$, 9.87 %ID/g; $[^{64}Cu\text{-}EPH270]^+$, 7.43 %ID/g), potentially due to the monocationic lipophilic nature of the complexes.

Overall tumor uptake for both complexes was higher at 4 and 24 h compared with values at 1 h, with $[^{64}Cu\text{-}EPH144]^+$ (1 h, 4.70 %ID/g; 4 h, 8.80 %ID/g; 24 h, 6.64 %ID/g) having greater accumulation and retention than $[^{64}Cu\text{-}EPH270]^+$ (1 h, 2.58 %ID/g; 4 h, 6.00 %ID/g; 24 h, 4.80 %ID/g). Although $[^{64}Cu\text{-}EPH144]^+$ at 24 h had the highest tumor activity, tumor-to-nontarget organ ratios for the liver, kidney, and muscle revealed similarity for the 2 agents at all time points. In particular, the tumor-to-muscle ratios were not significantly different ($P > 0.1$) at any time point examined (1 h, 2.29 $[^{64}Cu\text{-}EPH144]^+$ vs. 2.56 $[^{64}Cu\text{-}EPH270]^+$; 4 h, 5.48 $[^{64}Cu\text{-}EPH144]^+$ vs. 5.40 $[^{64}Cu\text{-}EPH270]^+$; 24 h, 4.95 $[^{64}Cu\text{-}EPH144]^+$ vs. 4.53 $[^{64}Cu\text{-}EPH270]^+$). The tumor-to-blood ratios for the agents did demonstrate a significant difference by 24 h ($P < 0.05$), with $[^{64}Cu\text{-}EPH144]^+$ showing consistently higher values (1 h, 0.94 $[^{64}Cu\text{-}EPH144]^+$ vs. 0.70 $[^{64}Cu\text{-}EPH270]^+$; 4 h, 2.18 $[^{64}Cu\text{-}EPH144]^+$ vs. 1.17 $[^{64}Cu\text{-}EPH270]^+$; 24 h, 2.58 $[^{64}Cu\text{-}EPH144]^+$ vs. 1.57 $[^{64}Cu\text{-}EPH270]^+$).

Small-Animal Imaging

Small-animal PET images of $[^{64}Cu\text{-}EPH270]^+$ were obtained in *nu/nu* mice bearing either 12-d L1210 or 21-d PC-3 tumors. Representative PET images and coregistered images (PET and high-resolution microCT) are shown in Figure 5A (L1210 bearing) and Figure 5B (PC-3 bearing). The images show that the L1210 tumors can be easily visualized at all time points, whereas the PC-3 tumors were more difficult to delineate. It was necessary to use high-resolution CT anatomic images and PET/CT coregistered images to localize the PC-3 tumors. SUV calculations (Fig. 6) show that the uptake and retention of the tracer in the tumor, liver, and kidney follow similar trends and relationships as those observed in the tissue distribution studies. The compounds demonstrated significant uptake in the L1210 tumor at 1, 4, and 24 h. The tumor uptake was dramatically reduced in animals that were preinjected with VP-16 (e.g., at 4 h, SUV [without VP-16] = 1.14 ± 0.18 vs. SUV [with VP-16] = 0.41 ± 0.07, $P < 0.01$). This indicated a Topo-II–mediated tumor uptake of $[Cu\text{-}EPH270]^+$. The SUVs of the PC-3 tumors were significantly lower than those of the L1210 tumors (e.g., at 4 h after injection, SUV [L1210] = 1.14 ± 0.18 vs. SUV [PC-3] = 0.60 ± 0.19, $P < 0.05$; at 24 h after injection, SUV [L1210] = 1.17 ± 0.12 vs. SUV [PC-3] = 0.42 ± 0.13, $P < 0.01$). This correlates with higher Topo-II expression of L1210 tumor compared with PC-3 tumor shown by western blot. VP-16 also reduced uptake of the tracer in the PC-3 tumor. However, because the PC-3 tumor uptake was already low, the reduction in tracer accumulation was not as significant as that of the L1210 tumor (e.g., at 1 h, SUV [without VP-16] = 0.45 ± 0.13 vs. SUV [with VP-16] = 0.29 ± 0.11, P = not significant [NS]; at 4 h, SUV [without VP-16] = 0.60 ± 0.19 vs. SUV [with VP-16] = 0.44 ± 0.20, P = NS). For both L1210 and PC-3 tumor-bearing mice, the uptakes in the liver and kidney were not significantly affected by VP-16 pretreatment (e.g., 4-h liver uptake of L1210 tumor-bearing mice, SUV [without VP-16] = 3.38 ± 1.20 vs. SUV [with VP-16] = 3.25 ± 1.27, P = NS; 24-h kidney uptake of PC-3 tumor-bearing mice, SUV [without VP-16] = 0.75 ± 0.16 vs. SUV [with VP-16] = 0.88 ± 0.16, P = NS).

DISCUSSION

PET is a noninvasive imaging technique that delineates physiologic processes, complementing the high-resolution anatomic images of MRI and CT that can reveal important information about location of disease. Physiologic information from PET can significantly aid the diagnosis of disease and help direct treatment for individual patients. The increasing availability and broader dissemination of positron-emitting nuclides of copper make these isotopes an attractive option on which to base new positron-emitting radiopharmaceuticals.

Of the 4 ligands examined in this study (EPH142, EPH143, EPH144, and EPH270), 3 have significantly

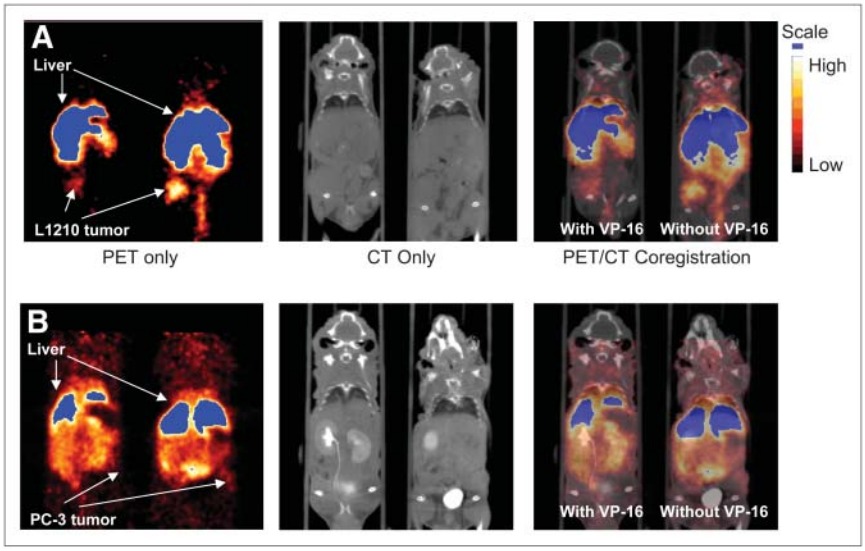

FIGURE 5. Images are 1-mm slices, with the animal in supine position, and slices are through the center of the tumor volume. Because tumors do not grow in exactly the same location from animal to animal, slices may show different tissues in addition to tumors. (A) Coronal images obtained using coregistration techniques demonstrating uptake of $[^{64}Cu\text{-}EPH270]^+$ at 4 h after injection into L1210 tumor implanted on the right flank of a mouse. The image on the left shows the mouse that received preinjection of VP-16. PET images show that administration of VP-16 substantially reduces tumor uptake of the agent to the extent that the tumor is difficult to delineate. The mouse on the right did not receive preinjection of VP-16 and this tumor had greater accumulation of radioactivity compared with the littermate on the left. (B) Coronal images of mice implanted with PC-3 tumors on the left flanks at 4 h after injection of $[^{64}Cu\text{-}EPH270]^+$. The PC-3 tumor is more difficult to delineate compared with the L1210 tumor. Image on the left, which shows the mouse that was pretreated with VP-16, demonstrates that the PC-3 tumor can barely be seen after administration of VP-16.

higher growth-inhibitory activities when complexed with nonradioactive copper (*29*): (IC_{50} values in HT29 cells: EPH142, 2.22 μmol/L vs. $[Cu\text{-}EPH142]^+$, 1.51 μmol/L; EPH144, 0.038 μmol/L vs. $[Cu\text{-}EPH144]^+$, 0.004 μmol/L; EPH270, 0.035 μmol/L vs. $[Cu\text{-}EPH270]^+$, 0.004 μmol/L) (*29*). Given the still-unfolding relationship between Topo-II and drug resistance, determining its clinical relevance might have significant impact on the treatment of patients. Here we describe the production and preliminary in vivo characterization of copper-radiolabeled analogs of Topo-II inhibitors (EPH142, EPH143, EPH144, and EPH270) as potential new radiopharmaceutical agents for delineating expression of Topo-II.

The 4 complexes were all produced in high radiochemical purity by the reaction of $^{64}CuCl_2$ with the ligand of choice in ethanolic solution. The radiolabeled complexes were characterized by both radio-TLC and radio-HPLC and shown to be identical in chemical form to the nonradioactive copper analogs. All 4 cationic complexes, of the general formula $[^{64}Cu(L)]Cl$, were lipophilic, with $[^{64}Cu\text{-}EPH144]^+$ the most lipophilic (logP = 1.92 ± 0.18).

Protocols for determining differential expression of Topo-II in various tumor lines using the Topo-II assay kit and western blot analysis were tested. In harvested tumor tissues, L1210 had the highest level of Topo-II, LL/2 and PC-3 had intermediate levels, with LL/2 levels of Topo-II slightly higher then those of PC-3, and MCF-7 had a relatively low level (Figs. 2A and 2B). When measuring tumor growth in animals, it was interesting to note that L1210 and LL/2 were rather aggressive tumors, PC-3 was somewhat less aggressive, and MCF-7 grew at a rather slow rate. This is consistent with the expression of Topo-II being a specific and sensitive marker for cell proliferation (*20,21*). Western blot of the cellular extracts from cultured cell lines (Fig. 2C) indicated that L1210 demonstrated the highest level of Topo-II protein, EMT-6, B16F10, and CaSki had intermediate levels, whereas the Topo-II levels of MCF-7 and PC-3 were the lowest and close to each

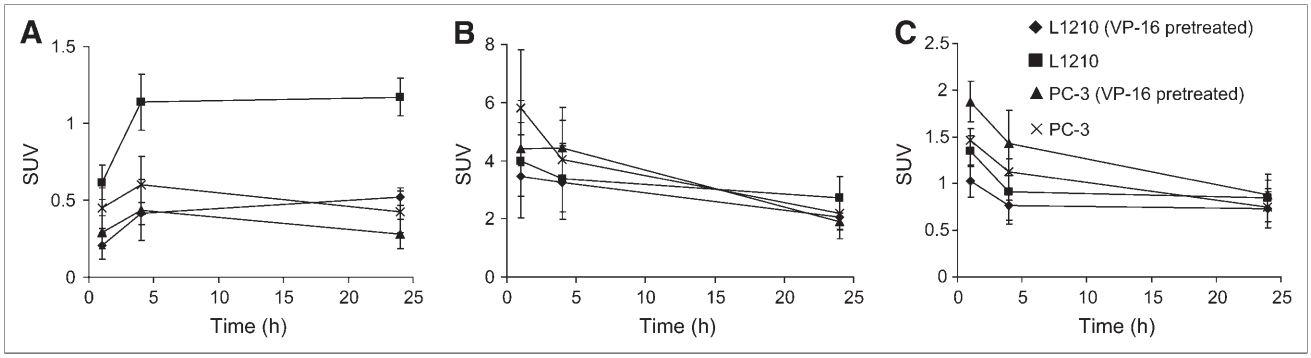

FIGURE 6. SUVs of uptakes of $[Cu\text{-}EPH270]^+$ in tumor (A), liver (B), and kidney (C) in L1210 and PC-3 tumor-bearing mice.

other, although MCF-7 showed a slightly higher Topo-II level. Western blots of the tumor extracts and cellular extracts showed a different order of Topo-II levels for MCF-7 and PC-3 cells, probably related to the different proliferation stages of the 2 cell lines in culture (*19–21*). VP-16 (etoposide), a Topo-II poison, inhibits the activity of Topo-II by stabilizing the cleavage complexes so that the enzyme does not regulate the DNA breaks (*37,38*). Using pure Topo-II and comparing its inhibition by VP-16 and by [Cu-EPH270]$^+$ demonstrated that [Cu-EPH270]$^+$ does inhibit Topo-II activity (Fig. 3), although its exact mechanism is yet to be determined.

The in vitro cell uptake study of [Cu-EPH270]$^+$ showed that as the mass of [Cu-EPH270]$^+$ added to the cells was increased internalization/binding increased in a dose-dependent manner until saturation was achieved. These observations strongly suggest that a process based on dose–response was responsible for the accumulation of the Cu-TSC into Topo-II–rich cells.

The 2 compounds with the highest logP values, [^{64}Cu-EPH144]$^+$ and [^{64}Cu-EPH270]$^+$, were chosen for further evaluation in vivo. Interestingly, the same 2 nonradioactive copper complexes were reported to have the most potent antitumor effects and the lowest IC_{50} values in HT29 cells (*29*). Because L1210, a lymphocytic leukemia–derived cell line, has high Topo-II expression in exponentially growing cells (*20,26*)—a finding confirmed in this current study—L1210 tumors were expected to express high levels of Topo-II and were selected for the in vivo tumor studies. Western blot of both tumor extracts and cell extracts showed that PC-3 has a significantly lower level of Topo-II compared with the L1210 cell line; therefore, we decided to use PC-3 tumors in the imaging studies for comparison. The L1210 tumor line and the PC-3 tumor line were also chosen for these studies because they are known to be drug sensitive and do not express P-glycoprotein, a potential complication in the study of lipophilic cationic complexes.

The biodistribution of [^{64}Cu-EPH144]$^+$ and [^{64}Cu-EPH270]$^+$ demonstrated high tumor uptake at 1 h after injection. In both cases, maximum tumor uptake was noted at 4 h. Our studies also revealed high nontarget tissue uptake—particularly, in the lung, heart, and spleen. It has been reported that Topo-II is abundant in the spleen of the adult mouse (*39*), explaining, in part, accumulation of the tracer in this tissue. Moreover, in humans, the tissues that contain the high amounts of Topo-II are the actively proliferating ones—germinating centers of lymphoid tissue, basal layers of epithelial and glandular tissue of colon, lung, and testis—whereas few scattered cells containing Topo-II have been detected in liver, kidney, and brain (*40*). This finding could explain the high uptake of the compounds in the lung. Topo-II levels have been shown to be low in the murine brain and the heart (*39*); therefore, the high heart uptake of the complexes can best be explained by the cationic and lipophilic nature of the complexes. Lipophilic monocations are known to enter cells by passive diffusion and to accumulate within cells—particularly, within mitochondria—as a result of the electrical potential gradient across the respective membranes in actively metabolizing cells (*41*).

It is evident from the PET studies that uptake in the kidney and liver is not significantly modulated by the administration of VP-16, suggesting that the Topo-II–dependent uptake of the agent in these tissues is likely to be minimal and is due to normal excretory processes. This is further supported by the fact that only a few scattered cells containing Topo-II have been detected in the liver and kidney (*40*). The uptake and subsequent retention in the kidney and liver also demonstrate minimal removal of the activity from the body, which could result in unacceptable dosimetry and low target-to-background ratios.

Although biodistribution studies demonstrated a less-than-favorable distribution of the tracers (i.e., high nontarget tissue accumulation) at all time points (1, 4, and 24 h), small-animal PET was able to delineate the L1210 tumors in the animal model. The SUV values were lower than those obtained in the biodistribution study but can be explained by the increase in the amount of compound (~30-fold) given in PET compared with that in the biodistribution study. The VP-16 studies provide evidence that an accumulation process associated with Topo-II expression may exist, as only tumor uptake was altered. It was not possible to use nonradioactive [Cu(EPH270)]$^+$ as a blockade because the insolubility of nontracer quantities of the complex does not allow for the administration of this compound to rodents. In all cases, the administration of VP-16 resulted in a significant reduction in overall L1210 tumor uptake without affecting the uptakes of the nontargeting organs such as liver and kidney. Compared with L1210 tumor, the PC-3 tumor was not easily visualized on the PET images and the PC-3 tumor uptakes at all time points were significantly lower than those of L1210 tumor, consistent with the lower Topo-II level of PC-3 cell line. With evidence that these compounds act against Topo-II, along with the high and low expression of Topo-II in the L1210 and PC-3 tumors, respectively, it is reasonable to hypothesize that the uptake and retention of these copper complexes is the direct result of a specific interaction with Topo-II.

This study investigated the radiolabeling and in vivo characterization of a new class of copper-radiolabeled TSC complexes. To the best of our knowledge this is also the first report of the use of PET radiopharmaceuticals as potential agents for delineating Topo-II expression in tumors. We have successfully produced these radiolabeled complexes and demonstrated that, despite high nontumor uptake, visualization of Topo-II–rich tumors can be accomplished with PET. Moreover, this accumulation can be significantly reduced with Topo-II inhibitors. Further studies are now warranted, including the design of new analogs to improve tumor uptake with a concomitant decrease in nontarget tissue accumulation.

CONCLUSION

This study describes new radiopharmaceuticals that may be useful for imaging Topo-II expression. We have demonstrated a proof of concept that these complexes are able to image the levels of cellular Topo-II. Although further translation of these four agents may be hindered by less-than-optimal background accumulation, this concept may help in the design and development of improved imaging and therapeutic agents targeted toward Topo-II.

ACKNOWLEDGMENTS

The authors gratefully acknowledge the help of Dr. Wenping Li for the HPLC analysis of the complexes. We thank Susan Adams, Lori Strong, Nicole Fettig, Margaret Morris, Dawn Werner, Jerrel Rutlin, Ann Stroncek, and John Engelbach for technical assistance. This work was financially supported by U.S. Department of Energy grant DE-FG02-87ER60512, and the production of ^{64}Cu was supported by National Cancer Institute (NCI) grant R24 CA086307. PET was supported by National Institutes of Health/NCI SAIRP grant 1 R24 CA083060, with additional support from the Small Animal Imaging Core (SAIC) of the Alvin J. Siteman Cancer Center at Washington University and Barnes-Jewish Hospital. The SAIC was supported by NCI Cancer Center Support grant 1 P30 CA091842.

REFERENCES

1. McCarthy DW, Bass LA, Cutler PD, et al. High purity production and potential applications of copper-60 and copper-61. *Nucl Med Biol.* 1999;26:351–358.
2. McCarthy DW, Shefer RE, Klinkowstein RE, et al. Efficient production of high specific activity ^{64}Cu using a biomedical cyclotron. *Nucl Med Biol.* 1997;24:35–43.
3. Haynes NG, Lacy JL, Nayak N, et al. Performance of a ^{62}Zn/^{62}Cu generator in clinical trials of PET perfusion agent ^{62}Cu-PTSM. *J Nucl Med.* 2000;41:309–314.
4. Blower PJ, Lewis JS, Zweit J. Copper radionuclides and radiopharmaceuticals in nuclear medicine. *Nucl Med Biol.* 1996;23:957–980.
5. Green MA. A potential copper radiopharmaceutical for imaging the heart and brain: copper-labeled pyruvaldehyde bis(N^4-methylthiosemicarbazone). *Int J Rad Instrum B*. 1987;14:59–61.
6. Taniuchi H, Fujibayashi Y, Yonekura Y, Konishi J, Yokoyama A. Hyperfixation of copper-62-PTSM in rat brain after transient global ischemia. *J Nucl Med.* 1997;38:1130–1134.
7. Young H, Carnochan P, Zweit J, Babich J, Cherry S, Ott R. Evaluation of copper(II)-pyruvaldehyde bis(*N*-4-methylthiosemicarbazone) for tissue blood flow measurement using a trapped tracer model. *Eur J Nucl Med*. 1994;21:336–341.
8. Dehdashti F, Grigsby PW, Mintun MA, Lewis JS, Siegel BA, Welch MJ. Assessing tumor hypoxia in cervical cancer by positron emission tomography with ^{60}Cu-ATSM: relationship to therapeutic response—a preliminary report. *Int J Radiat Oncol Biol Phys.* 2003;55:1233–1238.
9. Fujibayashi Y, Taniuchi H, Yonekura Y, Ohtani H, Konishi J, Yokoyama A. Copper-62-ATSM: a new hypoxia imaging agent with high membrane permeability and low redox potential. *J Nucl Med.* 1997;38:1155–1160.
10. Lewis JS, Sharp TL, Laforest R, Fujibayashi Y, Welch MJ. Tumor uptake of copper-diacetyl-bis(*N*^{4}-methylthiosemicarbazone): effect of changes in tissue oxygenation. *J Nucl Med.* 2001;42:655–661.
11. Lewis JS, McCarthy DW, McCarthy TJ, Fujibayashi Y, Welch MJ. The evaluation of ^{64}Cu-diacetyl-bis(*N*^{4}-methylthiosemicarbazone) (^{64}Cu-ATSM) in vivo and in vitro in a hypoxic tumor model. *J Nucl Med.* 1999;40:177–183.
12. Lewis JS, Herrero P, Sharp TL, et al. Delineation of hypoxia in canine myocardium using PET and copper(II)-diacetyl-bis(*N*^{4}-methylthiosemicarbazone). *J Nucl Med.* 2002;43:1557–1569.
13. Dehdashti F, Mintun MA, Lewis JS, et al. In vivo assessment of tumor hypoxia in lung cancer with ^{60}Cu-ATSM. *Eur J Nucl Med Mol Imaging.* 2003;30:844–850.
14. Lewis JS, Laforest R, Buettner TL, et al. Copper-64-diacetyl-bis(*N*^{4}-methylthiosemicarbazone): an agent for radiotherapy. *Proc Natl Acad Sci U S A*. 2001; 98:1206–1211.
15. Lewis JS, Connett JM, Garbow JR, et al. Cu-64-pyruvaldehyde-bis(N^4-methylthiosemicarbazone) for prevention of tumor growth at wound sites following laparoscopic surgery: monitoring therapy response with microPET and magnetic resonance imaging. *Cancer Res.* 2002;62:445–449.
16. Aft RL, Lewis JS, Zhang F, Kim J, Welch MJ. Enhancing targeted radiotherapy by copper(II)diacetyl-bis(N^4-methylthiosemicarbazone) using 2-deoxy-D-glucose. *Cancer Res.* 2003;63:5496–5504.
17. Larsen AK, Skladanowski A, Bojanowski K. The roles of DNA topoisomerase II during the cell cycle. *Prog Cell Cycle Res.* 1996;2:229–239.
18. Larsen AK, Gobert C, Gilbert C, Markovits J, Bojanowski K, Skladanowski A. DNA topoisomerases as repair enzymes: mechanism(s) of action and regulation by p53. *Acta Biochim Pol.* 1998;45:535–544.
19. Heck MM, Hittleman WN, Earnshaw WC. Differential expression of DNA topoisomerases I and II during the eukaryotic cell cycle. *Proc Natl Acad Sci U S A.* 1988;85:1086–1090.
20. Potmesil M, Hsiang Y-H, Liu LF, et al. Resistance of human leukemic and normal lymphocytes to drug-induced DNA-cleavage and low levels of DNA topoisomerase-II. *Cancer Res.* 1988;48:3537–3543.
21. Heck MM, Earnshaw WC. Topoisomerase II: a specific marker for cell proliferation. *J Cell Biol.* 1986;103:2569–2581.
22. Hwang JL, Shyy SH, Chen AY, Juan CC, Whang-Peng J. Studies of topoisomerase-specific antitumor drugs in human lymphocytes using rabbit antisera against recombinant human topoisomerase II polypeptide. *Cancer Res.* 1989;49:958–962.
23. Larsen AK, Escargueil AE, Skladanowski A. From DNA damage to G2 arrest: the many roles of topoisomerase II. *Prog Cell Cycle Res.* 2003;5:295–300.
24. Larsen AK, Escargueil AE, Skladanowski A. Catalytic topoisomerase II inhibitors in cancer therapy. *Pharmacol Ther.* 2003;99:167–181.
25. Isaacs RJ, Davies SL, Sandri MI, Redwood C, Wells NJ, Hickson ID. Physiological regulation of eukaryotic topoisomerase II. *Biochim Biophys Acta.* 1998;1400:121–137.
26. Doyle LA. Topoisomerase expression in cancer cell lines and clinical samples. *Cancer Chemother Pharmacol.* 1994;34(suppl):S32–S40.
27. Robert J, Larsen AK. Drug resistance to topoisomerase II inhibitors. *Biochimie.* 1998;80:247–254.
28. Robson CN, Hoban PR, Harris AL, Hickson ID. Cross-sensitivity to topoisomerase II inhibitors in cytotoxic drug-hypersensitive Chinese hamster ovary cell lines. *Cancer Res.* 1987;47:1560–1565.
29. Easmon J, Purstinger G, Heinisch G, et al. Synthesis, cytotoxicity, and antitumor activity of copper(II) and iron(II) complexes of ^{4}N-azabicyclo[3.2.2]nonane thiosemicarbazones derived from acyl diazines. *J Med Chem.* 2001;44:2164–2171.
30. Easmon J, Puerstinger G, Roth T, et al. 2-Benzoxazolyl and 2-benzimidazolyl hydrazones derived from 2-acetylpyridine: a novel class of antitumor agents. *Int J Cancer.* 2001;94:89–96.
31. Easmon J, Heinisch G, Holzer W, Rosenwirth B. Novel thiosemicarbazones derived from formyl- and acyldiazines: synthesis, effects on cell proliferation, and synergism with antiviral agents. *J Med Chem.* 1992;35:3288–3296.
32. Miller MC 3rd, Stineman CN, Vance JR, West DX, Hall IH. The cytotoxicity of copper(II) complexes of 2-acetyl-pyridyl-4N-substituted thiosemicarbazones. *Anticancer Res.* 1998;18:4131–4139.
33. Miller MC 3rd, Bastow KF, Stineman CN, et al. The cytotoxicity of 2-formyl and 2-acetyl-(6-picolyl)-4N-substituted thiosemicarbazones and their copper(II) complexes. *Arch Pharm (Weinheim).* 1998;331:121–127.
34. Chen J, Huang Y-W, Liu G, et al. The cytotoxicity and mechanisms of 1,2-naphthoquinone thiosemicarbazone and its metal derivatives against MCF-7 human breast cancer cells. *Toxicol Appl Pharmacol.* 2004;197:40–48.
35. Muller MT, Spitzner JR, DiDonato JA, Mehta VB, Tsutsui K, Tsutsui K. Single-strand DNA cleavages by eukaryotic topoisomerase II. *Biochemistry.* 1988;27:8369–8379.
36. Tai YC, Ruangma A, Rowland DJ, et al. Performance evaluation of the microPET Focus: a third-generation microPET scanner dedicated to animal imaging. *J Nucl Med.* 2005;46:455–463.
37. Burden DA, Kingma PS, Frolich-Ammon SJ, et al. Topoisomerase II·etoposide interactions direct the formation of drug-induced enzyme-DNA cleavage complexes. *J Biol Chem*. 1996;271:29238–29244.
38. Hande K. Etoposide is a topo-II poison, stabilizing transient covalent bond with DNA and promoting degradation and apoptosis. *Eur J Cancer.* 1998;34:1514–1521.
39. Juenke JM, Holden JA. The distribution of DNA topoisomerase II isoforms in differentiated adult mouse tissues. *Biochim Biophys Acta.* 1993;1216:191–196.
40. Turley H, Comley M, Houlbrook S, et al. The distribution and expression of the two isoforms of DNA topoisomerase II in normal and neoplastic human tissues. *Br J Cancer.* 1997;75:1340–1346.
41. Carvalho PA, Chiu ML, Kronauge JF, et al. Subcellular distribution and analysis of technetium-99m-MIBI in isolated perfused rat hearts. *J Nucl Med.* 1992;33:1516–1521.